Yeo, J.; Jin, H.; Rodrigo Mor, A.; Chau, Y.; Pattanadech, N.; Tushar, W.; Saha, TK.... (2023). Localisation of Partial Discharge in Power Cables Through Multi-Output Convolutional Recurrent Neural Network and Feature Extraction. IEEE Transactions on Power Delivery. 38(1):177-188. https://doi.org/10.1109/TPWRD.2022.3183588

Localisation of Partial Discharge in Power Cables Through Multi-Output Convolutional Recurrent Neural Network and Feature Extraction

J. Yeo, *Student Member, IEEE*, H. Jin, A. Rodrigo Mor, C. Yuen, *Fellow, IEEE,*
N. Pattanadech, W. Tushar, *Senior Member, IEEE*, T. K. Saha, *Fellow, IEEE,* and C. S. Ng

***Abstract*-- This paper proposes an algorithmic approach constructed from a convolutional recurrent neural network (CRNN) iterated with examination of extracted features for partial discharge (PD) localisation; tests were conducted offline on medium voltage (MV) power cables. To evaluate the performance of the algorithm, a case study was performed on 7 cables deliberately selected to comprehensively illustrate the difficulties encountered in field testing. The experimental test results prove that the proposed concept is able to identify and localise discharges besmirched with significant quantities of noise. Main contribution of the methodology is the successful automated interpretation of measurements acquired under noisy challenging field constraints.**

***Index Terms*—partial discharge, neural networks, medium voltage cables**

I. Introduction

Partial discharge diagnostic test in medium-voltage cables are commonly used in modern electrical networks to identify incipient faults in the material, preventing material degradation from prolonged PD occurrence. The typical problems faced during offline measurements are on-site noise and the large quantities of collected data – this consequently requires highly skilled operators and considerable amount of evaluation time. Automatic evaluation first and foremost requires a highly accurate identification procedure ensuring that the number of false positives (FP) and false negatives (FN) are as little as possible. Subsequently, a robust localisation procedure that is not susceptible to the unavoidable noise influence in order to process the discharge location with high accuracy is needed.

All PD measurements systems, online or offline, are dependent on some form of digital mechanisation, which have mainly been rule-based systems. Whilst these systems provide a degree of automation, practitioners in the field are aware that relying completely on human-crafted rules do not provide the dependability for noise-induced PD measurements. This is because given the intricate temperament of the waveforms, if-then rules may be inconsistent – the same antecedent may map to different consequents. On-site noise when combined with the variety seen on field measurements i.e., length of cable, number of joints, and mixed insulation system leads to an infinite possibility of arrangements that cannot be determined comprehensively by conventional curated rule sets. Machine learning (ML) and deep learning (DL), on the other hand, offers an alternative approach – the difference is that data-based design is probabilistic in nature and can resolve categorisation conflict raised from deterministic rules. The application of DL on PD is not new – the first exploration dates back to approximately thirty years ago [1] [2] [3]. With the exponential progress seen recently on computational progress and advancement in DL capabilities, PD recognition experiences a revitalisation on the topic of application with DL techniques.

Recent research on ML/DL related PD localisation has been focused on all aspects of electrical equipment – transformers, switchgears, cables and even substation itself, however not much effort is focused on cables [4]. In [5], to localise PD in power transformers, a nonlinear neuro-fuzzy localisation system using unsupervised pattern recognition combined with feature vectors was proposed – the proposed method was based on a localisation system with rules created from the relationship of input signal features. Experimental results in the laboratory showed significant improvement in localising major types of PD when compared to techniques available then. In [6], to localise PD in gas insulated switchgears, time-frequency analysis, edge detection and support vector machine was proposed to identify longitudinal and circumferential position of PD source – the proposed method extract features from received signals for entry into both an algorithm and a ML model. Experimental results from the simulation and laboratory were successful, with no errors made for circumferential

J. Yeo is with the Engineering Product Development pillar, Singapore University of Technology and Design, Singapore (joel_yeo@mymail.sutd.edu.sg).
H. Jin is with T Yeo Engineers Pte. Ltd., Singapore (hfj@tyeoengineers.com).
A. Rodrigo Mor is with Universitat Politècnica de València, Instituto de Tecnología Eléctrica, Valencia, Spain (arrodmor@ite.upv.es).
C. Yuen is with the Engineering Product Development pillar, Singapore University of Technology and Design, Singapore (yuenchau@sutd.edu.sg).
N. Pattanadech is with Faculty of Engineering, Electrical Engineering Department, King Mongkut's Institute of Technology Ladkrabang, Bangkok, Thailand. (norasage.pa@kmitl.ac.th)
W. Tushar is with the School of Information Technology and Electrical Engineering, University of Queensland, Queensland, Australia (w.tushar@uq.edu.au).
T. K. Saha is with the School of Information Technology and Electrical Engineering, University of Queensland, Queensland, Australia (saha@itee.uq.edu.au).
C. S. Ng is with T Yeo Engineers Pte. Ltd., Singapore (csng@tyeoengineers.com).

localisation accuracy. In [7], to localise PD in substation, a wavelet packet transform extracted features and an ensemble learning method with regression tree, bootstrap, aggregating and random regression forest was proposed. Attention to corruption by noise was addressed through wavelet package transformation. The authors acknowledge the interference between an electrical substation and confines of a laboratory are dissimilar, but affords reasonable complexity for the purpose of simulation. Experimental results showed localisation accuracy to be high, with low variance of location error. In [8], to localise time resolved PD (TRPD) in cables, relevant parameters of events are extracted. Applying rule-based classification and pairing, statistical ratings are generated categorising the likelihood of a discharge and corresponding location. Evaluation here is based on the experience of field testing, where it was concluded that inaccurate exact localisation of key parameters could lead to wrong conclusions.

As described, for localisation of PD, the combination of machine-driven interpretation and manual feature selection has proven to be successful when used in tandem. There has not been a DL study conducted on localising TRPD measurements performed on in-service MV cables from offline test. Currently, there is no solution to fully computerise evaluation efforts with a high degree of certainty on the discharge location without human intervention. Autonomous and confident localisation is essential in MV cable diagnosis, in order to reduce operator workload and handle large amounts of unknown data.

Computational analysis of PD in cable measurements is in two distinct but correlated parts – identification and localisation. To address the impediment arising from noise and complications in field measurements, an iterative algorithm comprised from neural networks (NNs) and PD features are presented; this paper accretes on the previous work from PD identification performed in [9] and complements with localisation of the discharge positions – demonstration will be shown on 7 case studies of varying complexion. In [9], PD identification methodology was proposed with transfer learning and NN ensembles that differentiates between PD and noise on individual cables.

Introduced in this paper is the identification and localisation of TRPD measurements. Expanding on the predicted PD output of [9], through application of a multi-output CRNN, localisation of one PD direct (PDD) and five first reflection (FR) pulse positions can be acquired. In addition to knowledge of the pulse locations, PD identification improvement can be effectuated by applying a threshold rule on the PDD pulse extracted features – normalised cumulative summation (CS) orders 2 and 3. Thereafter, one FR pulse will be selected through feature examination on the pulse polarity, peak and area of the initial five FR pulses. For PD identification, to corroborate the improvement, distinction is made between results obtained through the methodology from [9] and the approach from this paper – emphasis is placed on the reduction of FPs. For PD localisation, to evince the attributes of feature analysis, comparison is made between the FR localisation results from the standalone CRNN and from the proposed feature extraction and heuristics – emphasis is placed on the accuracy increment. For clarity, identification in this paper describes identification between PD and noise, localisation describes locating the PDD and FR discharge pulse positions.

The framework overview for the multi-step methodology is as follows sequentially, creation of a PD databank used to train the CRNN, identification between PD and noise through [9], data segmentation on predicted PDs via sliding window principle for a frame-by-frame scrutiny to localise a singular PDD and five FR pulses, perform PD identification by feature analysis on the localised PDD position therein reducing FPs, thereafter selection of FR location through examination of features within proposed sliding window. In order to exhibit the robustness of this algorithm, a performance evaluation is conducted through 7 case studies to elucidate the applicability.

The structure of the paper is as follows – Section II introduces the background of the study, Section III proposes the algorithm of the experimental work, Section IV describes the results of the methodology and finally Section V summarises for conclusion.

II. Background Information

A. Partial Discharge Fundamentals

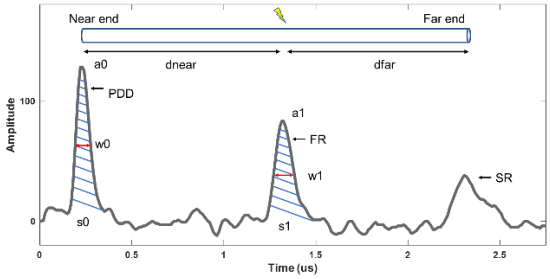

Fig. 1. Classical three-pulse signature of PD measurement in cable, with annotations for feature extractions.

Shown in Fig. 1 is the classical signature of a TRPD measurement caused by a single PD source in an offline PD cable test. The measurements are subjected to signal attenuation, as illustrated with the three decaying pulses – PDD, FR and second reflection (SR); the time difference between PDD and FR informs the discharge location. The other annotations in Fig. 1 will be explained in the subsequent section.

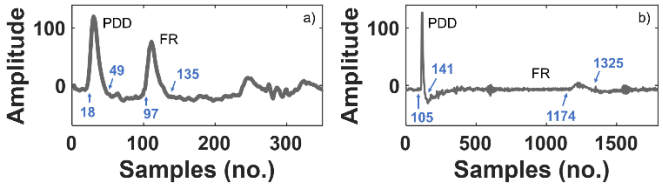

Fig. 2. PD measurements with indices for knee-point of pulses; (a) Short cable, (b) Long cable.

Due to dispersion in the frequency spectrum, the PD pulses tend to be wider as they travel along the cable; this is observed more prominently for longer cables. Shown on the left in Fig. 2a, it can be noted that the knee-point of PDD and FR for the shorter cable is less than 50 samples, with FR being slightly wider than PDD. Shown on the right in Fig. 2b is a measurement on a longer cable with discharge location close to the near end. It can be seen that the knee-point for the FR pulse of the longer

cable differs significantly, PDD is narrow whereas the width of FR is much wider; the pulse is almost 150 samples wide. Undoubtfully, this has an effect during numerical processing which must be addressed accordingly with appropriate selection tools.

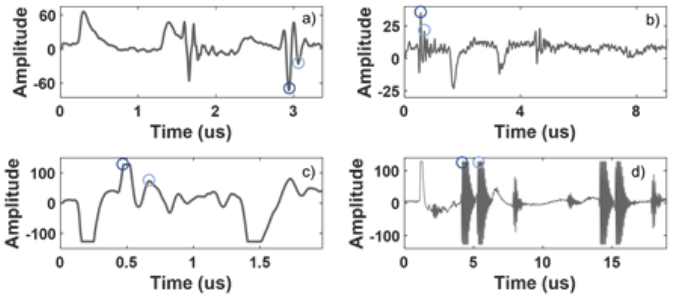

Fig. 3. PD pulses measured with different noise influences, (a) Non-stationary noise, (b) High frequency noise, (c) Low frequency noise, (d) Repetitive noise.

Noise interference in field testing is unavoidable and could originate both internally and externally [10]. It could be non-stationary as shown in Fig. 3a, with constant repetition as shown in Fig. 3d, or with high and low frequencies as shown in Fig. 3b and c respectively. Therefore, when utilising computational analysis for localisation of the PDD and FR pulses, it is important to consider the exposure to noise from the field and PD pulse behaviours exhibited under non-ideal conditions. Circled in dark and light blue at different points within Fig. 3a to d are examples of simple algorithmic approach which considers the largest amplitude and finds a succeeding pulse of a similar polarity – dark blue circle represents PDD pulse, light blue circle represents FR pulse. From the given plots in Fig. 3, it is possible to apprehend the difficulties posed from field measurements; Fig. 3a to d are examples of some waveforms which bear similarity to our case studies that will be presented later.

B. Feature Extraction for Partial Discharge

TABLE I
Common PD Features

Variables	Physical Description
a0	Magnitude of PD direct
a1	Magntitude of 1st reflection
dnear	Distance of PD event to cable near end
dfar	Distance of PD event to cable far end
r0	Rise time of PDD pulse
f0	Fall time of PDD pulse
s0	Area of PDD pulse
s1	Area of FR pulse
w0	Width at half maximum of PDD pulse
w1	Width at half maximum of FR pulse
CS1	$CS1(i) = \frac{\sum_1^i x_i}{\sum_1^N x_i}$, cumulative summation order 1
CS2	$CS2(i) = \frac{\sum_1^i x_i^2}{\sum_1^N x_i^2}$, cumulative summation order 2
CS3	$CS3(i) = \frac{\sum_1^i x_i^3}{\sum_1^N x_i^3}$, cumulative summation order 3

Shown in Table I are the common feature extractions [11] performed on PD pulses to obtain a quantitative representation during computational recognition purposes – physical descriptions of the variables from Table I are illustrated in Fig. 1. Typically, algorithms are designed to identify points of interest through consideration and correlation of numerous predetermined variables. However, whilst such descriptions are meaningful in a controlled environment i.e., laboratory conditions, there are difficulties when translating to field measurements; moreover, extraction of these features also depends heavily on the correct manual selection. Majority of the conventional factors such as magnitude and time interval of the pulses, rise and fall time of PDD pulse, distance of PD event with respect to cable ends, width at half maximum of the PDD and FR pulse provides little distinction when compared with noise signatures. Furthermore, some form of selection tool needs to be deployed in order to extract the features.

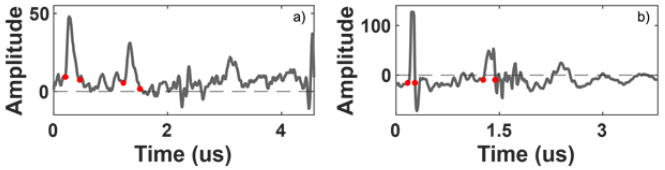

Fig. 4. Imperfect PD field measurements, (a) Positive DC offset, (b) Negative DC offset.

Examples of other imperfect field measurements can be seen in Fig. 4, the zero-crossings of the PDD and FR pulses are dotted in red. Plotted on the left in Fig. 4a, positive non-constant offset caused the pulse to not have any zero-crossings; and on the right in Fig. 4b with a negative offset, zero-crossings which are not at the knee-point of the pulse. If not accounted for, these factors will have misleading influences during feature extracting calculations. In order to identify points of interest, it is clear that a selection tool is imperative. Addressing once more the aforementioned conventional factors in the previous paragraph, given the different amplitudes received in each measurement, it is apparent that certain conventional factors are unable to provide discrimination between PD and noise. For instance, the magnitude of the PDD pulse in Fig. 4a is equivalent to the magnitude of the FR pulse in Fig. 4b – noticeably, consideration of such arbitrary values without contextual information do not offer any definitive insight.

C. Sliding Window Method

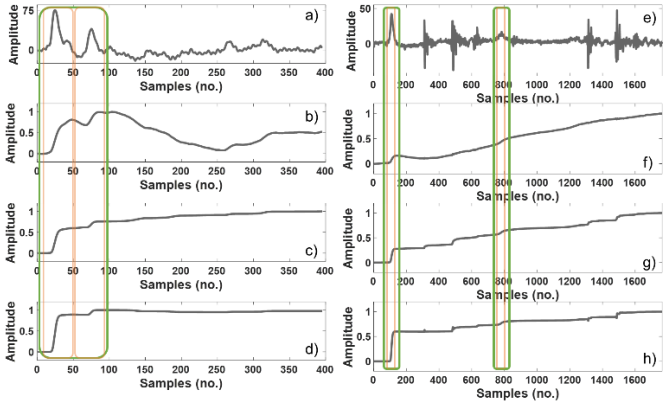

Fig. 5. PD measurement in cable and subsequent normalised CS of different orders, (a) PD measurement in short cable, (b) CS order 1 of (a), (c) CS order 2 of (a), (d) CS order 3 of (a), (e) PD measurement in long cable, (f) CS order 1 of (e), (g) CS order 2 of (e), (h) CS order 3 of (e).

As stated earlier, in order to extract features of interest, some form of selection tool is crucial. In this paper, application of sliding windows is proposed, the window is fixed in length and slides over the array while computing statistic of the data at

each step. Shown on the top in Fig. 5a and e are windows of two different lengths – 50 and 100 samples long, in orange and green respectively; the differentiation is to accommodate differing pulse sizes. As shown in Fig. 5a, it can be seen for the shorter cable, a smaller window would register only the pulse of interest, whereas the larger window has the likelihood of recording additional unwanted signals; as shown in Fig. 5e, it can be seen that the converse holds true for longer cables. Compared to Fig. 5a, the FR pulse in Fig. 5e is much wider and requires a larger window; smaller window would not encapsulate the entire pulse. In this paper, the decision between using a smaller or a larger sliding window size depends on the number of samples in each waveform. For waveforms with less than 1000 samples a smaller window is used, whereas for waveforms with more than 1000 samples a larger window is used.

Parameters of potential suitability from application of sliding windows are area of pulses and the CS of the waveforms in different orders – as these elements indirectly relate to the change in energy witnessed during a PD event. Shown in the preceding three waveforms of Fig. 5a and e are increasing orders of normalised CS for the respective waveforms. It can be observed from the first order in Fig. 5b and f, which indirectly relates to the integral of the waveform, that noise segments are relatively constant, whereas the PD pulse will cause an increase in area as discharges contain charge. It can be observed from the second and third orders in Fig. 5c, d, g and h, while certain noise perturbation also causes some fluctuation, there is a prominent change at the position of a discharge.

For further identification of PD, the normalised CS of order 2 and 3 is examined on the suggested location of the PDD pulse. For selection of the FR pulse, the integral of the waveform is examined on the suggested locations of FR positions.

It is evident that the success for feature extraction is highly dependent on the correctly chosen window size. While such a task is elementary for a human operator, it is challenging for conventional rule-based systems due to the convoluted nature of field measurements. Therefore, highly accurate NN is employed to propose sliding windows of interest in order to perform feature extraction for identification and localisation.

D. Neural Network Fundamentals

Detailed description of various relevant NNs and working principles [12] [13] [14] has been written in previous works [15] [16]. In this paper, only two NNs will be used in different arrangements for the identification of PD and localisation of pulse position – convolutional neural network (CNN) and recurrent neural network with either long short-term memory (LSTM) cells or bidirectional long short-term memory (BILSTM) cells. For the identification of PD and noise, CNN and BILSTM is used in an ensemble as described in [9]. For the localisation of pulse position, the CNN and LSTM are used in a multi-output CRNN architecture.

Shown in Fig. 6 is a CRNN architecture, where the input consists of several arbitrary channels, these channels are processed by two-dimension convolution window of fixed size. The sliding window moves in steps and outputs the convolution of the input data. Max pooling followed by average pooling is performed, to initially pick up the strongest features followed by smoothing out the values. The data is cascaded to LSTM cells, where the temporal dependencies are captured, and finally sent to two separate dense layers.

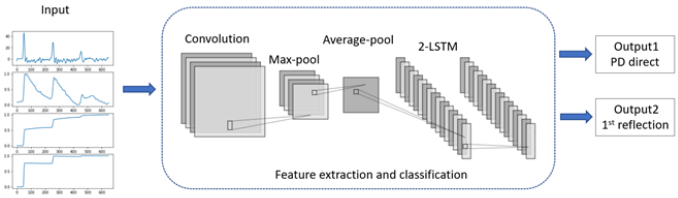

Fig. 6. CRNN model architecture.

For a multi-output classification network, two sets of fully-connected dense layers need to be present for the respective outputs – in this case, the PDD and FR; each dense layer is responsible for localisation of the respective discharge position.

In totality, the input of the multi-output CRNN proposed in this paper accepts an arbitrary number of inputs and outputs the location of the PDD and FR; the architecture of the CRNN will be detailed in the following chapter.

E. Data Set for Partial Discharge Identification and Localisation

TABLE II
Data Set Size and Distribution

	[9]	Localisation
Data Set Size	47852	16710
PD vs Noise	50%-50%	100%-0%
Max. Waveform Length	2560 samples	

The PD localisation data set, as shown on the right of Table II, used for training the NN is a subset of the data set derived from [9] – detailed description for the original data set has been given therein. The original data set, which have all been manually labelled, is composed solely of offline MV cable measurements obtained from in-service cables. Data set from [9] was evenly distributed between PD and noise, while the localisation data set is only made up of PD. The data set size in the localisation data set is not half of the original data set – this is because further curation was done with the purpose of only using distinct and diverse PD signatures with a balanced bias for more advantageous training. The localisation data set was divided between training and validation samples by a 9:1 ratio. As the training of a NN is a stochastic process, training and validation results were the average of ten iterations, with each iteration consisting of 50 epochs.

Similar to [9], the NNs were then tested on individual case studies that are not included in the database. They were deliberately selected to illustrate a range of different conditions faced in the field for demonstration capability of the proposed method.

III. Methodology

A. Proposed Algorithm

Shown in Fig. 7 is the formulation for the proposed algorithm of this paper. Development of the CRNN model is as shown above the dotted line of Fig. 7, with results of the designed model discussed subsequently in Subsection IV.B.

The localisation and identification process are as represented below the dotted line of Fig. 7.

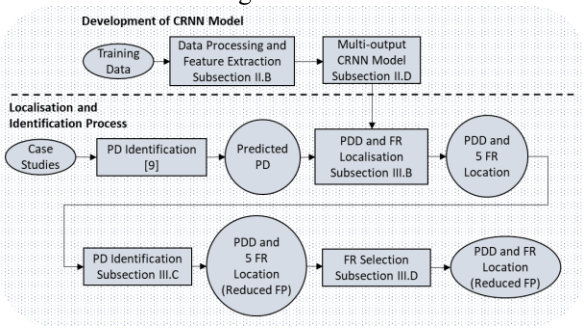

Fig. 7. Proposed algorithm flowchart, with according explanation in the respective subsections.

The case study measurements are inputted to the algorithm of [9] which outputs predicted PD and noise. Predicted noise samples are discarded, while predicted PD – containing both true and false positives, are cascaded to the localisation and identification process; small amounts of unwanted FPs are resultant from the transfer learning process introduced in [9].

Normalised CS of orders 1, 2 and 3 are performed on each waveform and along with the original waveform are inputted to the multi-output CRNN. The convolutional section of the CRNN processes the input with the sliding window method, concatenating to the LSTM cells after, which then outputs the location of the PDD and FR pulses. Further identification of PD is effectuated on the predicted PD data through feature analysis at the PDD location – this sieves out FPs. Thereafter, selection of FR location is made through conditions imposed on features from multiple suggested FR locations. Succeeding subsection will explain the concept of the intended objectives for further PD localisation and identification.

B. Partial Discharge Direct and First Reflection Localisation

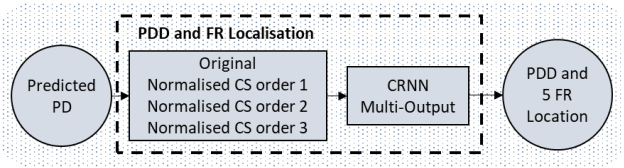

Fig. 8. PDD and FR localisation, with feature extraction before NN analysis.

The PD localisation algorithm used in this paper utilises feature extraction before and after NN analysis. The segment concerned with the PDD and FR pulse localisation is expanded in Fig. 8. The original signal, along with the normalised CS of orders 1, 2 and 3 are entered to the multi-output CRNN, as shown in Fig. 8 – the multiple waveforms are inputted to the proposed CRNN architecture as shown in Table III.

Four inputs are entered into the CRNN and two-dimension convolution is performed through a sliding window, which moves in steps to process the data. Batch normalisation is performed to stablise the NN by re-centering and re-scaling, followed by max pooling, which reduces the dimensionality and focuses on key features. Average pooling merges all the four inputs to be processed by LSTM cells, which have long-term dependencies learning properties. Experiments between both LSTM and BILSTM cells have been made and it was discovered that while the latter is more computationally

TABLE III
Topology of CRNN

Layers	Output shape	Parameter	Connected to
Input	(4, 2560)	0	
Reshape_1	(4, 2560, 1)	0	Input
Conv2d	(4, 247, 128)	12928	Reshape_1
Batch normalisation	(4, 247, 128)	512	Conv2d
Max pooling	(4, 123, 128)	0	Batch normalisation
Average Pooling	(1, 123, 128)	0	Max pooling
Reshape_2	(123, 128)	0	Average Pooling
LSTM_1	(123, 64)	49408	Reshape_2
LSTM_2	(123, 64)	33024	LSTM_1
Dropout	(123, 64)	0	LSTM_2
Flatten	(7872)	0	Dropout
Dense (PDD output)	(256)	2015488	Flatten
Dense (FR output)	(256)	2015488	Flatten

Total parameters: 4,126,848
Trainable parameters: 4,126,592
Non-trainable parameters: 256

intensive, it is not advantageous. Dropout layer prevents overfitting through regularisation. Finally, the output is decided through a softmax function from the dense layer. The two dense layers are not connected together, but instead receives the input in parallel from the flatten layer as can be seen from Table III – the two different layers correspond to the localisation of the PDD and FR pulse positions respectively. Trainable parameters refer to parameters that optimises itself with the training data, whereas non-trainable parameters are parameters that will not be updated during the training, i.e., the moving mean and moving variance parameters within batch normalisation.

For the algorithm in this paper, the output of the CRNN results in a singular PDD location and five FR locations. The PDD localisation has been found to be highly accurate and is accepted; it can also be used for further identification purposes to reduce the amount of FPs, as will be explained in the following subsection. Five FR locations are further analysed and compared with various features and conditions, as it has been found that a high percentage of the correct location is not from the largest valued suggestion of the softmax output but instead within the first five largest valued suggestions. The objective in this segment is to localise the PDD position and also five FR pulse positions.

C. Partial Discharge Identification

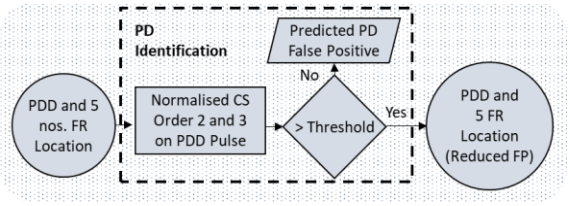

Fig. 9. Analysis of PDD pulse features for increasing identification accuracy.

The algorithm used in the initial PD analysis stages is explained thoroughly in [9], difficulty in PD and noise separation from field measurements are well described in the entry. In this paper, only the CNN and BILSTM NNs in *Ensemble 2* will be used, as it had the best fully automated result. Introduction of transfer learning at the initial analysis stage in [9] was able to reduce the amount of FNs but at the expense of increased FP.

The segment concerned with PD identification from Fig. 7 is expanded in Fig. 9. During the experimental stages of the localisation algorithm, it was discovered that the accuracy for locating the PDD pulse is generally close to 100%. This gave the confidence to rely on the predicted PDD location, and numerically observe stepwise changes for presence of discharge in the normalised CS orders 2 (which indirectly indicates energy) and 3, as explained earlier in Fig. 5. Waveforms with normalised CS orders 2 or 3 exceeding a threshold in the given sliding window location are accepted as PD; the converse holds true. The threshold was set at 0.25.

The objective in this segment is to reduce FPs from the initial identification process through scrutiny of the PDD pulse – the output is predicted PDs with reduced FPs and the subsequent location of the PDD pulse. Result observation for this introduction focuses on the reduction of FPs.

D. First Reflection Selection

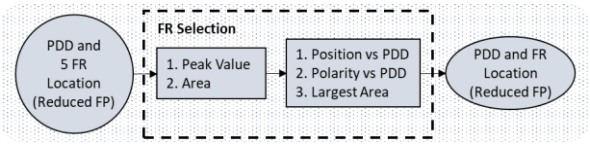

Fig. 10. Analysis of FR pulse features with conditions to select position.

Not all waveforms from the output of Fig. 8 are conveyed for analysis in Fig. 10 as some FPs are excluded due to the PD identification procedure performed in Fig. 9. Through the previous assay in Fig. 8 and Fig. 9, the resultant input to Fig. 10 is a set of predicted PDs with reduced FPs, and a confirmed PDD location – which is important as it acts as a mainstay for conditional selection of the FR pulse.

The features and conditions for selecting the correct FR location are as given below,

1. Remove predictions in vicinity of PDD location.
2. Remove predictions if polarity for PDD and FR peak value and area are dissimilar.
3. Select largest area from remaining predictions.
4. In the event there is no remaining predictions due to mismatched conditions, reinstate first original prediction.

The validity and success of the imposed conditions is vastly contingent on the PDD pulse; which alludes that if the PDD localisation is incorrect, there will be a cascading effect.

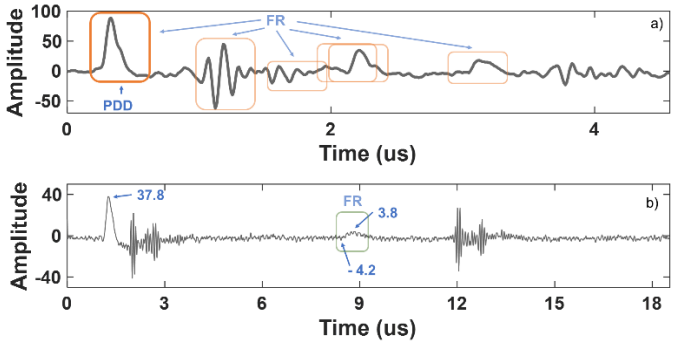

Fig. 11. Localisation of PD and FR pulses through CRNN, (a) Example of outputs, (b) Example of anomaly.

An example of the proposed evaluation through the conditions is as shown in Fig. 11a. The CRNN indicates several probable FR discharge locations, it can be recognised that through the appropriate selection of features and imposed conditions to analyse, it is achievable to localise the correct FR pulse, which is slightly after 2 us.

In principle, the aforementioned first three conditions should suffice. However, shown in Fig. 11b is an example of an anomaly, where due to the irregularities of field measurement, abnormalities occurred and required invoking condition 4. The PDD peak was 37.8 units in amplitude, whereas the absolute largest FR value within the sliding window was not 3.8 units in amplitude at the peak of the FR pulse, but is -4.2 units in amplitude at the left knee-point of the pulse, due to a mild offset of the waveform – this resulted in a positive area but a negative peak value, violating condition 2 when comparing with the PDD pulse. In this rare situation (four waveforms within all the case studies), selection of the original prediction will be made.

The objective in this segment is to select a FR pulse location – to demonstrate the accuracy of our proposed algorithm, comparison of results between the algorithm and solely the multi-output CRNN will be made.

E. Data Processing

Given a limited data set, data augmentation is performed to increase the amount of data through modifying existing copies. For the context of our data structure and principle, reversing of the waveform polarity is the only applicable transformation.

As the input to the NN must be similar, waveforms are commonly extended using various approaches – zero, repeated or mean padding. For the context of PD measurements, zero-padding is the only applicable modification.

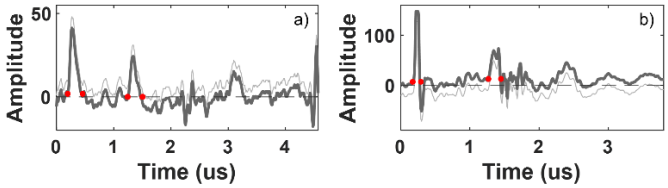

Fig. 12. Normalisation of waveform, (a) Positive offset, (b) Negative Offset.

Explained in earlier sections, field tests are susceptible to erratic conditions resulting in unpredictable measurements. Normalisation of the waveform is required due to compounding effect it causes otherwise during feature extraction; in this paper, the offset is compensated through the mean value of the first ten samples. As shown in Fig. 12a, the positive offset in Fig. 4a is reduced, and shown in Fig. 12b, the negative offset in Fig. 4b is neutralised. Noticeable in both plots from Fig. 12, this compensation is possible even for non-constant gain values and presents a good approximation.

In the context of feature extraction, as shown previously in Fig. 5a, for a short cable, if a larger sliding window is used, excessive considerations are made, as shown in Fig. 5e, for a long cable, if a smaller sliding window is used, incomplete capture of the pulse is made – it can be understood that consideration of the wrong sliding window length will result in the incorrect misinterpretation for the points of interest.

IV. Experimental Results

A. Case Study

The 7 cable case studies will be described next, with the x-axis of the plots in samples instead of time, for correlation to the length of the sliding window – orange windows are 50 samples long, whilst green windows are 100 samples long; waveforms lesser than 1000 samples use a smaller window, whilst waveforms greater than 1000 samples use a larger one. The description for presentation is as follows – amount of total recording, distribution between PD and noise, number of discharge spots on the cable, length of samples in the TRPD waveforms, selected size of sliding window, location for end of cable, information on the FR location, and a characterisation of the case study. As mentioned earlier, the 7 case studies constitute of in-service cables taken offline and tested at various voltage levels, selection of the cables were deliberate to comprehensively delineate the difficulties encountered in field testing. The compilation consists of short and long cables, between two to four pulses, which were besmirched with fluctuating and irregular noise patterns. All the files have been manually labelled to distinguish between PD and noise – within each PD waveform manual labelling has also been performed for the location of the PDD and FR pulse; this is drawn accordingly on the plots with sliding window of the appropriate size.

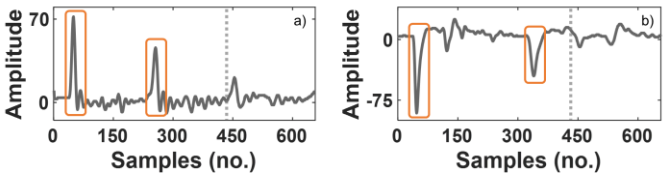

Fig. 13. *Cable 1*, uncomplicated three-pulse measurement from short cable, (a) First discharge location before sample no. 300, (b) Second discharge location after sample no. 300.

Cable 1 had 387 recordings, composed of 385 PD and 2 noise waveforms, had 2 discharge spots, recorded waveforms were 659 samples long as shown in Fig. 13. As shown on the plot, window of 50 samples long would be more suitable to contain the pulse instead of a larger window; the end of the cable is as denoted with the dotted vertical line. The first discharge spot can be seen from Fig. 13a positioned before sample no. 300, and the second can be seen from Fig. 13b positioned after sample no. 300. This is a typical three-pulse measurement and is uncomplicated as the signal-to-noise (SNR) ratio for the FR pulse was large.

Cable 2 had 407 recordings, composed of 277 PD and 130 noise waveforms, had 3 discharge spots, recorded waveforms were 1045 samples long as shown in Fig. 14, with a sliding window of 100 samples long being used; the end of the cable is as denoted with the dotted vertical line. Due to the close proximity of the 3 discharge spots, the discharge location is denoted on the plots in Fig. 14 for demarcation – the first discharge has the peak centered approximately at sample no. 555, as shown in Fig. 14a and c, the second and third discharge is around sample no. 496 and 634, as shown in Fig. 14b and d respectively. This is a three-pulse measurement for a longer cable, with the FR attenuated and dispersed. The FR pulse is much smaller in amplitude compared to the PDD pulse and the measurement contains high frequency noise.

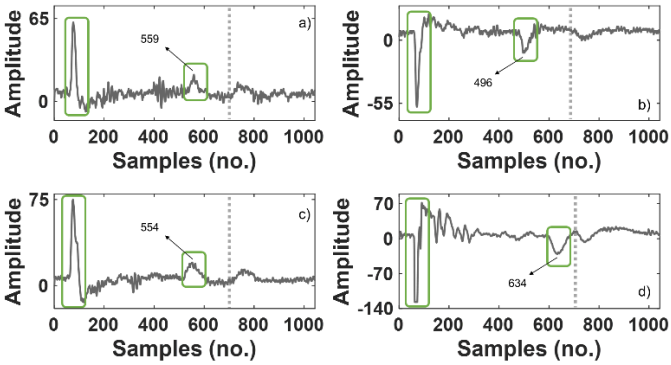

Fig. 14. *Cable 2*, three-pulse measurement from long cable, (a) and (c) First discharge location at approximately sample no. 555, (b) Second discharge location at sample no. 496, (d) Third discharge location at sample no. 635.

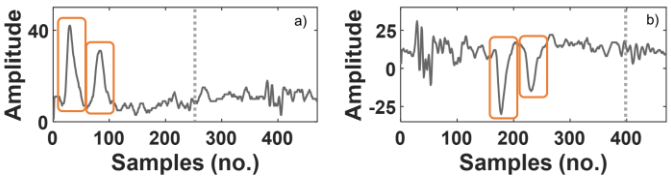

Fig. 15. *Cable 3*, two-pulse measurement from short cable, (a) Correctly triggered recording, (b) Incorrect triggered recording result in excessive pre-trigger measurement.

Cable 3 had 228 recordings, composed of 173 PD and 55 noise waveforms, had 1 discharge spot, recorded waveforms were 470 samples long as shown in Fig. 15, with a sliding window of 50 samples long used here; the end of the cable is as denoted with the dotted vertical line. This is a discharge located on the far end of the cable, evident firstly from the closeness between the two pulses, and also through the increase in pulse width – indicative of dispersion as the pulse travels along the cable. This is a two-pulse measurement, with a large FR pulse, and consisted of low and high frequency noise. The measurement also suffered from occasional wrong triggering, with excessive pre-trigger measurements, which caused the PDD pulse to be shifted later in samples to an uncommon position – this unusual PDD position is a good assessment to validate the generalisation behaviour of the CRNN, to see if the NN is able to recognise an unexpected PDD position.

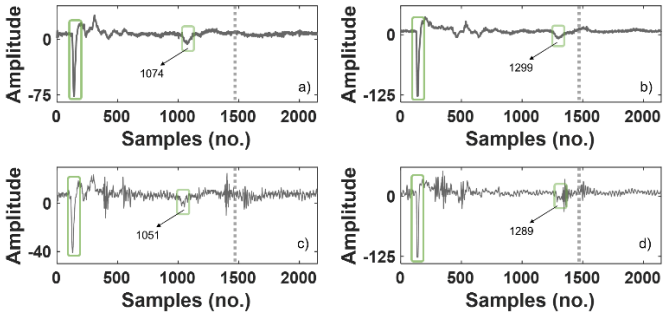

Fig. 16. *Cable 4*, two-pulse measurement from long cable, (a) and (c) First discharge location, (b) and (d) Second discharge location.

Cable 4 had 551 recordings, composed of 78 PD and 473 noise waveforms, had 2 discharge spots, recorded waveforms were 2147 samples long as shown in Fig. 16, with a sliding

window of 100 samples long being used; the end of the cable is as denoted with the dotted vertical line. As shown in Fig. 16a for the first discharge location, with relatively no noise disturbance, it is clear that the attenuated FR pulse poses some challenge in recognition. In Fig. 16c, with increased presence of noise disturbance, the FR pulse is almost indistinguishable amidst the larger surrounding interference. Similar sequence of events is observed for the second discharge location with Fig. 16b and d; with Fig. 16d almost unrecognisable when superimposed by an external noise influence. This is a two-pulse measurement from a long cable, and a complicated file as there is poor SNR; it is a file of interest for analysis.

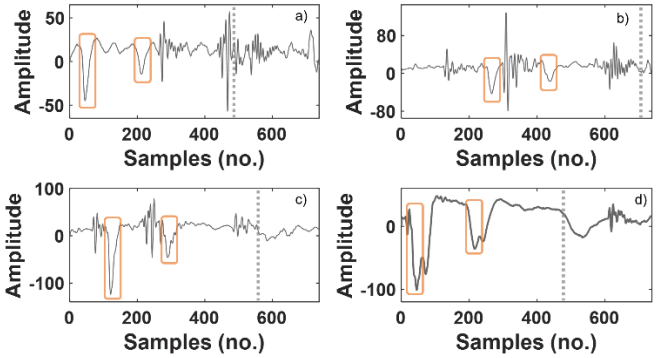

Fig. 17. *Cable 5*, two-pulse noisy measurement from short cable, (a) External noise larger than PD signal, (b) Excessive pre-trigger and large external noise, (c) Slight time-shifted recording, (d) Multiple fused discharges.

Cable 5 had 304 recording, composed of 113 PD and 191 noise waveforms, had 1 discharge spot, recorded waveforms were 740 samples long as shown in Fig. 17, with a sliding window of 50 samples long being used; the end of the cable is as denoted with the dotted vertical line. Shown in Fig. 17a to d, it can be observed that the PDD pulse does not keep to a regular position, but instead is traversing along the measurement due to erroneous triggering of the recording. Evident in Fig. 17a to c, the measurement is polluted with repetitive noise of amplitudes larger than the PD pulses; in Fig. 17a some noise oscillations bear resemblance to PD signatures. Occasionally, as plotted in Fig. 17d, there are discharge pulses fused together – an infrequent albeit noteworthy manifestation. Similar to *Cable 3,* this unusual roving PDD pulse is a good assessment of the CRNN generalisation behaviour. This is a two-pulse measurement in a short cable with large external noise disturbance; a complicated file which is of interest for analysis.

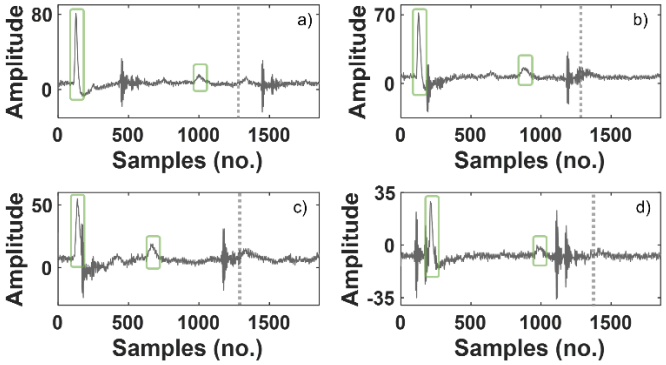

Fig. 18. *Cable 6*, two-pulse noisy measurement from long cable, (a) to (c) Examples of 3 different discharge locations, (d) Similar discharge location compared to (b) but shifted in time.

Cable 6 has 193 recording, composed of 177 PD and 16 noise waveforms, had 5 discharge spots, recorded waveforms were 1854 samples long as shown in Fig. 18, with a sliding window of 100 samples long being used; the end of the cable is as denoted with the dotted vertical line. Shown in Fig. 18a to c are 3 examples of the discharge locations; Fig. 18d is the same discharge location as Fig. 18b, but shifted in samples due to an erroneous trigger on the large noise spike before the PDD pulse. Comparable to *Cable 4* and 5, this measurement is also polluted with repetitive noise of amplitudes larger than the FR pulse, and the FR pulse greatly attenuated and almost unrecognisable. This is a two-pulse measurement in a long cable with large external noise disturbance, and a complicated file which is of interest for analysis.

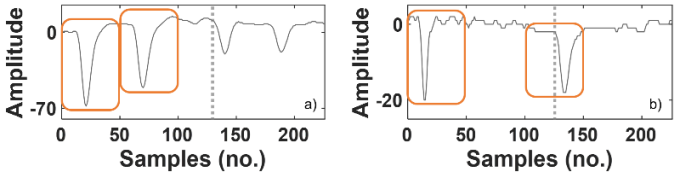

Fig. 19. *Cable 7*, four-pulse measurement, (a) First discharge location, (b) Second discharge location.

Cable 7 has 239 recording, composed of 217 PD and 22 noise waveforms, had 2 discharge spots, recorded waveforms were 228 samples long as shown in Fig. 19, with a sliding window of 50 samples long being used; the end of the cable is as denoted with the dotted vertical line. This is an unusual four-pulse measurement, caused by incorrect input cable length value during initial testing stage, resulting in excessive recording. The measurement contains a non-constant offset as shown in Fig. 19b, which presents difficulties in conventional interpretation. Shown in Fig. 19a is the first discharge location and in Fig. 19b is the second discharge location. Given known details about end of the cable it is presumed the source of the discharge for Fig. 19b to be close to the terminations. This file is of interest for analysis.

TABLE IV
Case Study Summary.

Cable	Recordings	Discharge Spots	Sample Length	Sliding Window Size
1	387	2	659	50
2	407	3	1045	100
3	228	1	470	50
4	551	2	2147	100
5	304	1	740	50
6	193	5	1854	100
7	239	2	228	50

A summary of the case studies is as described in Table IV. As illustrated, the selection is considerable and extensive, it contained cables of short and long lengths, with small and large amounts of noise, and made up of two, three and four pulses. While the goal of the algorithm is to generalise well to unseen data, it is neither possible nor the purpose of the paper to present an exhaustive demonstration. Instead, common and unique measurements are shown, with multiple discharge locations and cable lengths, to expound the versatility of the algorithm performance.

B. Training and Validation Accuracy

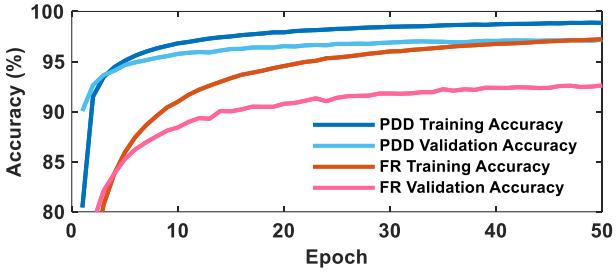

Fig. 20. Training and validation accuracy of PDD and FR pulses.

Shown in the Fig. 20 is the training and validation accuracy of the CRNN for both the PDD and FR pulse. This is the result for 10 iterations of 50 epochs. It can be seen that the stability of the results is reached by 40 epochs and therefore 50 epoch is sufficient. The validation accuracy of the PDD is slightly above 95%, while the FR is at approximately 90%. However, of importance is the performance of the NNs on unseen data.

C. Partial Discharge Identification

TABLE V
PD Identification Results Before and After Feature Consideration.

Cable	Acc (%)	Pre (%)	Rec (%)	TP	TN	FP	FN
1	98.97	100	98.96	381	2	0	4
	98.97	100	98.96	381	2	0	4
2	97.05	95.85	100	277	118	12	0
	98.28	97.54	100	277	123	7	0
3	86.84	87.43	96.53	167	31	24	6
	92.54	93.82	96.53	167	44	11	6
4	99.64	97.5	100	78	471	2	0
	100	100	100	78	473	0	0
5	90.46	80	99.12	112	163	28	1
	95.72	93.86	94.69	107	184	7	6
6	100	100	100	177	16	0	0
	97.41	100	97.18	172	16	0	5
7	95.4	95.58	99.54	216	12	10	1
	99.58	100	99.54	216	22	0	1

Shown in Table V is the PD identification result before and after proposed feature consideration on the PDD pulse – the intention is to address the PD identification improvement between [9] against the proposed method of Section III.B and Section III.C. For each respective case study, results before are on the top row and results after are on the bottom row. Accuracy (Acc), precision (Pre) and recall (Rec) are the standard statistical evaluation parameters derived from the confusion matrix values – true positive (TP), true negative (TN), FP and FN; these values are written to visibly portray the improvements.

As mentioned earlier, application of transfer learning in [9] has the advantage of increasing the accuracy and recall at the expense of reducing the precision – increase in FPs. Through the review on the CS of either the second or third order, it is propounded that the FPs can be reduced. Observation is made for the decrement in FPs, negative implication of unwanted increase in FNs, and overall accuracy performance.

Shown for *Cables 2*, *3*, *4*, *5*, and *7*, deliberation of the features generated an overall reduction of the FPs, as highlighted in dark grey, and enhanced the accuracy and precision scores – all identification accuracies are greater than 92%. *Cable 1* was not affected by the procedure, whereas a slight increase in FNs for *Cables 5* and *6* are visible as highlighted in light grey. Although *Cable 5* had an increase in FN, the accuracy was not affected as the improvement was greater.

Shown earlier in Fig. 5 are two waveforms, which contained visible change in amplitude at suggested PDD location, the changes corresponded to locations where there were discharges. Shown here in Fig. 21a and e are noise waveforms but were both wrongly identified as PD by the analysis from [9].

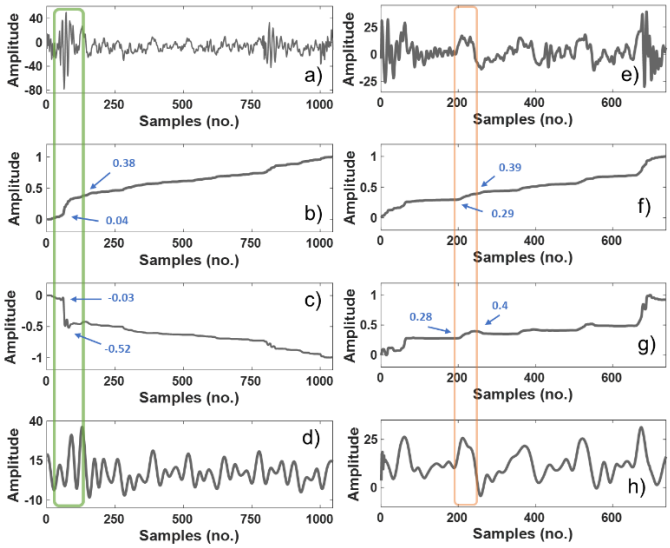

Fig. 21. FP waveforms in (a) and (e), Normalised CS order 2 and 3 in (b), (c), (f) and (g), DWT plot in (d) and (h).

The suggested PDD position is as given, and both contained a change in amplitude in normalised CS order 2 and 3 within the frame. Shown on Fig. 21a is a noise measurement from *Cable 2*, from a theoretical point of view, it would be difficult to say this is a PD; performing manual assessment via discrete wavelet transform (DWT) [17] as shown in Fig. 21d with wavelet Daubechies 16 at a threshold of four decomposition levels do not reproduce any palpable content. As the normalised CS order 2 and 3 exceeded the threshold of 0.25, as shown in Fig. 21b and c, this waveform remained mistakenly identified as PD after both the analysis from [9] and feature consideration on the PDD pulse – for any methodology it is expected that there will be outliers to the results. Shown on Fig. 21e is a noise measurement from *Cable 5*, whilst it comprised of questionable peaks and troughs, there are no absolute factors that would confidently allow an operator to affirm this waveform as a PD. Given the complexity of the waveform, performing DWT with the same wavelet as before with similar four decomposition levels on the waveform do not show any prominent PD pulses as plotted in Fig. 21h. As neither the normalised CS order 2 or 3, as shown in Fig. 21f and g, exceeded the threshold of 0.25, whilst the waveform was mistakenly identified as PD during the analysis from [9], feature consideration on the PDD pulse successfully corrected the FP to a TN.

Overall performance of the proposed enhancement is notable – in context of the number of reduced FPs and increased accuracy and precision scores; only *Cable 6* suffered slightly in performance.

D. Partial Discharge Localisation

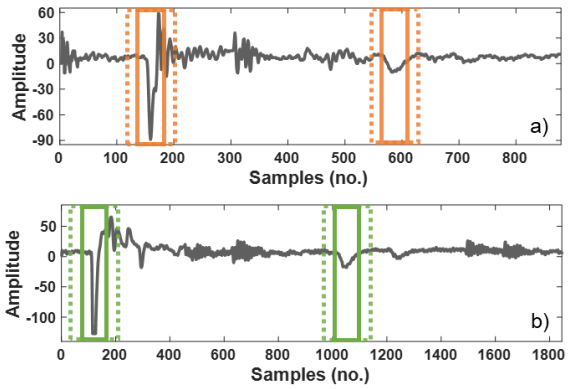

Fig. 22. Tolerance for localisation of PDD and FR pulses, (a) Short cable with sliding window 50 samples long, (b) Long cable with sliding window 100 samples long.

Shown in Fig. 22 is the tolerance for accepting the correct predicted PDD and FR position; the solid line box in both plots is the labelled pulse position, centered around the peak. The maximum tolerance for a short cable with sliding window 50 samples long is +/- 20 samples, and for a long cable with sliding window 100 samples long is +/- 40 samples. Shown in Fig. 22a with the dotted box is an illustration of the tolerance at the maximum of +/-20 samples for both the PDD and FR pulse – it can be seen that the selected tolerance is not inordinate. Similarly for Fig. 22b with the dotted box is the illustration of the tolerance at the maximum of +/-40 samples; it can be seen that the increased tolerance for a longer cable is felicitous and not disproportionate.

TABLE VI
FR Localisation Results Before and After Feature Consideration

Cable	PDD (%)	FR (%)		Noise
		Before	After	
1	100	100	99.47	0
2	100	97.47	99.64	7
3	100	100	100	11
4	100	71.79	96.15	0
5	100	96.46	99.12	7
6	99.43	81.35	94.35	0
7	99.53	99.53	100	0

Shown in Table VI is the localisation accuracy addressing the improvement between the standalone CRNN against the complete algorithm, which includes the feature extraction and Section III.D heuristic – the purpose of the comparison is to exemplify the efficacy of the supplementary arithmetic. The accuracy scores are shown for the PDD and FR pulses, noise represents the amount of FPs that were cascaded wrongly to the localisation algorithm alongside the TPs; the localisation algorithm takes in all predicted PDs – this comprises of both TPs and FPs. Similar to Table V, for Table VI highlighted in dark grey is improvement, while light grey is deterioration. Of interest, as mentioned earlier during the description of the case studies, are *Cables 4, 5, 6* and *7* due to the complicated and convoluted nature of disruptions in field measurements.

It is evident from the PDD pulse results that the CRNN can localise the position on its own accord; this was expected as primarily the PDD pulse is distinctive enough and thus usually unmistakable even if polluted by noise disturbance.

Localisation for TRPD pulses in cables has always been focused on the accuracy for recognising the FR pulse. For *Cables 1*, *2* and *3*, during relatively uncomplicated measurements, the NN is competent to recognise the position unassisted as proven from the high accuracies. For the remaining complicated measurements, the NN is still able to accomplish exceptional results on *Cables 5* and *7*. From the introduction of supplementary features and imposed conditions, *Cables* 2, *4*, *5*, *6* and *7* displayed improvements. Considerable advancement was achieved for *Cables 2*, *4*, *5* and *6,* whereas *Cable 7* had marginal improvement.

For *Cable 4*, the conglomerate of an almost diminished FR pulse adjacent with noise spikes caused ineffective recognition. However, approximately 25% increase in accuracy was gained through the additional feature considerations. For *Cable 5*, the NN independently performed well against this measurement that contained multiple complications i.e., small PD amplitude, incorrect recordings, low signal to noise ratio; further refinement to the evaluation elevated the accuracy. *Cable 6* was a longer cable with identical surrounding circumstances to *Cable 5*, using the additional feature considerations, almost 15% increase in accuracy was acquired.

Cables 1 and *3* did not show any improvement, with *Cable 1* decreasing slightly in FR localisation accuracy.

Validation scores for PDD and FR pulses were initially at approximately 95% and 90% respectively. The NN was capable of localising the PDD position autonomously, as proven with the accuracies consistently greater than 99%. Heuristics from the proposed algorithm was able to improve and generalised well on unseen data, with FR localisation accuracies between 94% to 100%. As seen from the overall results of Table VI, it can be concluded that the multi-output CRNN is competent, and that additional features and conditions is efficacious.

E. Further Analysis I – Discharge Localisation in Complex Waveforms

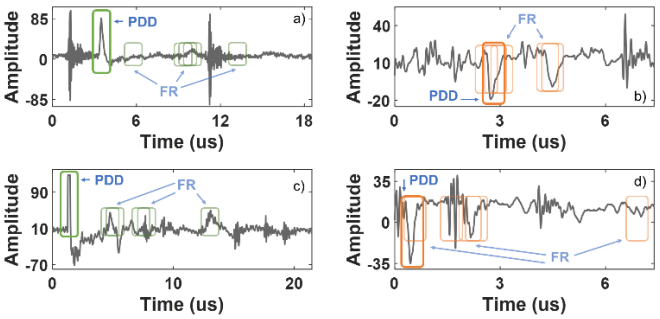

Fig. 23. Examples of complicated waveforms, (a) *Cable 6*, (b) *Cable 5*, (c) *Cable 4*, (d) *Cable 5*.

Shown in Fig. 23 are four correctly localised measurements that present difficulty in conventional analysis – time-shifted PDD pulse, noise perturbations being larger in amplitude than PD pulses, diminutive FR pulse, noise events that appear similar to PD events, and general poor overall SNR. Predictions from the NN are given in sliding windows of the dimensions proposed earlier; the PDD and FR pulses are as circumscribed accordingly within each plot. As mentioned earlier, there is the

possibility that the predictions for the FR pulse could fall in the position of the PDD and hence must be discarded – shown Fig. 23b and d are such examples.

For Fig. 23a, despite being hindered by noise that is larger in amplitude and earlier in time-axis, the NN is fully capable of localising both the PDD and FR position. Through the multiple FR predictions, it can be evidenced that with the proposed features and conditions, it is possible to select the right location even though the pulse is minuscule.

For Fig. 23b, the waveforms contained a DC offset, which coupled to noise events caused excessive pre-trigger recording and magnitudes larger than the PD pulses. Despite these hinderances, the NN is still able to localise the PDD pulse. There were several suggestions of the FR location in the vicinity of the PDD pulse which were incorrect and excluded through condition 1. Thereafter, correct localisation of the discharge position was made, despite an unremarkable pulse signature.

For Fig. 23c, the waveform has a prominent PDD pulse but consequently contained noise events that can easily be mistaken as FR pulses. Whilst the correct FR pulse is visible to the human eye, numerically the amplitude is comparable to the noise disturbances – this confusion can be seen through the multiple predictions made on the other positions containing spikes. Nonetheless, through the conditions imposed on the features, it is possible to select the correct FR location.

For Fig. 23d, the received signal is weak in magnitude and corrupted with large amounts of noise. The FR pulse is positioned adjacent to a sizeable noise event, which makes for an interesting investigation. Incorrect FR suggestion at the vicinity of the PDD pulse is algorithmically removed through invoking condition 1, with the remaining predictions assessed by conditions 2 and 3. Here, the functionality of the proposed extracted features can be witnessed. Given the multiple selections, it is clear that the FR pulse before the 3 us mark will be chosen, as neither the large noise perturbation on the left nor the small crest on the right will be larger in area.

All four waveforms were correctly localised, this unequivocally ascertains that proper consideration of the PD signature properties will enable correct recognition.

F. Further Analysis II – Incorrect Localisation of PDD Pulse

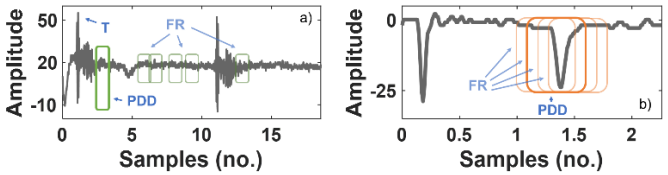

Fig. 24. Examples of incorrect localisation of PDD pulse position, (a) *Cable 6*, (b) *Cable 7*.

Shown in Fig. 24a and b are incorrect localisation of the PDD pulse position. In general, as seen from the accuracy of the algorithm, such occurrences are rare due to the inherent highly accurate PDD pulse localisation. In Fig. 24a, the recording was wrongly triggered on the noise spike denoted T, which had a positive peak of slightly over 50 units – this recorded an incomplete PDD pulse; there is also an offset seen constantly throughout the waveform of nearly 20 units large. The five FR outputs from the NN in Fig. 24a did not contain the correct position of the FR pulse, so imposed conditions on the features will not yield consequential results – this FR pulse localisation was incorrect. In Fig. 24b, the NN predicted the wrong PDD position, placing it on the FR location; this then nullified all the suggested FR positions through condition 2. Invoking condition 4, the first suggestion of the FR is reinstated, which was the correct location of the FR pulse; the PDD pulse was wrongly localised.

V. Conclusion

This paper investigates into identification and localisation of TRPD measurements from in-service MV cables and proposes an algorithm that iterates between feature extraction and NN. The presented methodology is able to identify and localise highly challenging PD waveforms found in field measurements. Comprehensive demonstration was performed on seven case studies, which were of different lengths and complexities. Success of the algorithm builds on highly accurate NNs to further enhance the generalisation capabilities on unseen data through deliberation of several relevant PD characteristics.

In consideration of the attenuation and dispersion the PD pulse suffers when travelling along the cable, appropriately sized sliding windows are essential for localisation of discharge positions. Inadequately sized windows do not allow full capture of the pulse, and on the other hand, excessively framed windows capture undue information. Therefore, when incorrect window size is applied, subsequent feature extraction do not produce meaningful results.

Selective conventional PD features has found to be effective – mainly parameters which are resilient to noise; a common predicament in field measurements. Normalised CS of different orders have found to be useful in both training of NNs and assisting evaluation thereafter. Both normalised CS order 1 and 2 are effective information as it indirectly relates to the charge and energy of a PD pulse.

For PD identification, through the combination of both feature extraction and NNs, identification accuracy and precision of the model have been increased, evaluation parameters which were diminished slightly by transfer learning from [9]. For PD localisation, the polarity and peak of the FR pulse value, along with the approximated area through integral of the data within the sliding window provided valuable navigation to the correct FR position, improving results compared to a standalone CRNN.

Through the proposed methodology it has been substantiated that identification and localisation of PDs are achievable and undeterred in noisy circumstances. The proposed algorithm exemplifies a logical, iterative, and uncomplicated DL approach towards identification and localisation of PD pulses. This approach is considered to be an instrumental and effective contribution to the topic of automated evaluation for TRPD in offline MV cable tests. With the results in this paper showing promise, future work will revolve around verifying the effectiveness in real world deployment.

VI. References

[1] H. Suzuki and T. Endoh, "Pattern Recognition of Partial Discharge in XLPE Cables Using a Neural Network," in *Proceedings of the 3rd International Conference on Properties and Applications of Dielectric Materials*, Tokyo, 1991.

[2] G. Katsuta, H. Suzuki, H. Eshima and T. Endoh, "Discrimination of Partial Discharge from Noise in XLPE Cable Lines Using a Neural Network," in *Proceedings of the Second International Forum on Applications of Neural Networks to Power Systems*, Yokohama, 1993.

[3] N. Hozumi, T. Okamoto and T. Imajo, "Discrimination of Partial Discharg Patterns Using Neural Network," in *Proceedings of the 3rd International Conference on Properties and Applications of Dielectric Materials*, Tokyo, 1991.

[4] J. Long, X. Wang, W. Zhou, J. Zhang, D. Dai and G. Zhu, "A Comprehensive Review of Signal Processing and Machine Learning Technologies for UHF PD Detection and Diagnosis (I): Preprocessing and Localization Approaches," *IEEE Access,* vol. 9, pp. 69876 - 69904, 2021.

[5] M. Homaei, S. M. Moosavian and H. A. Illias, "Partial Discharge Localization in Power Transformers Using Neuro-Fuzzy Technique," *IEEE Transactions on Power Delivery,* vol. 29, no. 5, pp. 2066 - 2076, 2014.

[6] X. Li, X. Wang, A. Yang and M. Rong, "Partial Discharge Source Localization in GIS Based on Image Edge Detection and Support Vector Machine," *IEEE Transactions on Power Delivery,* vol. 34, no. 4, pp. 1795 - 1802, 2019.

[7] E. T. Iorkyase, C. Tachtatzis, I. A. Glover, P. Lazaridis, D. Upton, B. Saeed and R. C. Atkinson, "Improving RF-Based Partial Discharge Localization via Machine Learning Ensemble Method," *IEEE Transactions on Power Delivery,* vol. 34, no. 4, pp. 1478 - 1489, 2019.

[8] D. Götz, F. Petzold, H. Putter, S. Markalous and M. Stephan, "Localized PRPD Pattern for Defect Recognition on MV and HV Cables," in *2016 IEEE/PES Transmission and Distribution Conference and Exposition (T&D)*, Dallas, 2016.

[9] J. Yeo, H. Jin, A. Rodrigo Mor, C. Yuen , W. Tushar, T. K. Saha and C. S. Ng, "Identification of Partial Discharge Through Cable-Specific Adaption and Neural Network Ensemble," *IEEE Transactions on Power Delivery,* 2021 (Accepted for publication).

[10] A. Rodrigo Mor, L. C. Castro Heredia and F. A. Munoz, "Estimation of Charge, Energy and Polarity of Noisy Partial Discharge Pulses," *IEEE Trans. Dielectr. Electr. Insul. ,* vol. 24, no. 4, pp. 2511-2521, 2017.

[11] N. Morette, T. Ditchi and Y. Oussar, "Feature Extraction and Ageing State Recognition Using Partial Discharges in Cables Under HVDC," *Electric Power Systems Research,* vol. 178, 2020.

[12] D. H. Hubel and T. N. Wiesel, "Receptive Fields and Functional Architecture of Monkey Striate Cortex," *The Jour. of Phys.,* vol. 195, no. 1, pp. 215-243, 1968.

[13] D. E. Rumelhart, G. E. Hinton and R. J. Williams, "Learning Representations by Back-Propagating Errors," *Nature,* vol. 323, pp. 533-536, 1986.

[14] S. Hochreiter, *Untersuchungen zu dynamischen neuronalen Netzen,* Munich: TUM.University Press, 1991.

[15] J. Yeo, H. Jin, C. Yuen and C. S. Ng, "Application of Recurrent Neural Network with Long Short-Term Memory Cells on Partial Discharge Identification," in *JICABLE'19 - 10th International Conference on Insulated Power Cables*, Versailles, 2019.

[16] J. Yeo, H. Jin, C. Yuen and C. S. Ng, "Developing Neural Network Models for Partial Discharge Analysis," in *IECON 2020 The 46th Annual Conference of the IEEE Industrial Electronics Society*, Singapore, 2020.

[17] J. Yeo, H. Jin, C. Yuen and C. S. Ng, "Predicting of Partial Discharge in Medium-Voltage Cables Using Recurrent Neural Network with Long Short-Term Memory Cells after Wavelet Denoising," in *2020 8th International Conference on Condition Monitoring and Diagnosis (CMD)*, Phuket, 2020.